© 2025 Journal of Pharmacy & Pharmacognosy Research, 13 (s1), S371-S393, 2025
ISSN 0719-4250
https://jppres.com

DOI: https://doi.org/10.56499/jppres25.2531_13.s1.371

Original Article

Profiling and potential of *Marchantia paleacea* Bertol. extract for breast anticancer candidate: GC-MS, LC-MS/MS, and *in silico* analysis

[Perfil y potencial del extracto de *Marchantia paleacea* Bertol. como candidato contra el cáncer de mama: GC-MS, LC-MS/MS y análisis *in silico*]

Etti S. Siregar[1*], Putri C. Situmorang[1], Nursahara Pasaribu[1], Hestia Hairima[2], Mufida R. Hasibuan[3]

[1]Department of Biology, Faculty of Mathematics and Natural Sciences, Universitas Sumatera Utara, Medan, Indonesia.
[2]Department of Biology, Faculty of Mathematics and Natural Sciences Universitas Negeri Medan, 20221, Indonesia,.
[3]School of Veterinary Medicine and Biomedical Science, Bogor Agricultural University, IPB Dramaga Campus-Bogor 16880, Indonesia.
*E-mail: etti1@usu.ac.id

Abstract

Context: Breast cancer remains a leading cause of cancer-related mortality among women worldwide. Limitations in existing targeted therapies, including resistance, toxicity, and cost, have renewed interest in plant-derived metabolites as potential breast anticancer agents. *Marchantia paleacea*, a liverwort species, represents an underexplored source of bioactive compounds with possible therapeutic relevance.

Aims: To characterize the phytochemical profile of *M. paleacea* and predict the breast anticancer potential of its metabolites through integrated chromatographic and computational approaches.

Methods: Metabolites were identified using gas chromatography–mass spectrometry (GC–MS) and liquid chromatography–tandem mass spectrometry (LC–MS/MS). Identified compounds were evaluated *in silico* for biological activity, drug-likeness, and target-binding affinity using PASS Online, Protox-3, SwissADME, and molecular docking analyses.

Results: Eighteen GC–MS and forty-eight LC–MS/MS metabolites were identified, including luteolin 7-O-glucuronide, baicalein 6-glucuronide, and dihydroresveratrol. These compounds exhibited favorable predicted antineoplastic and pro-apoptotic activities, as well as stable binding affinities toward HER2, caspase-3, and caspase-8 targets.

Conclusions: This *in silico* investigation highlights *M. paleacea* as a promising source of breast anticancer candidates. The findings warrant future *in vitro* and *in vivo* validation to substantiate their therapeutic potential.

Keywords: caspase; HER2; *Marchantia paleacea*; molecular docking; natural product drug discovery; phytochemical profiling.

Resumen

Contexto: El cáncer de mama sigue siendo una de las principales causas de mortalidad por cáncer entre las mujeres en todo el mundo. Las limitaciones de las terapias dirigidas existentes, incluida la resistencia, la toxicidad y el costo, han renovado el interés en los metabolitos derivados de plantas como posibles agentes anticancerígenos de mama. *Marchantia paleacea* representa una fuente poco explorada de compuestos bioactivos con posible relevancia terapéutica.

Objetivos: Caracterizar el perfil fitoquímico de *M. paleacea* y predecir el potencial anticancerígeno de mama de sus metabolitos mediante enfoques cromatográficos y computacionales integrados.

Métodos: Los metabolitos se identificaron mediante cromatografía de gases-espectrometría de masas (GC-MS) y cromatografía líquida-espectrometría de masas en tándem (LC-MS/MS). Los compuestos identificados se evaluaron *in silico* para determinar su actividad biológica, semejanza con los fármacos y afinidad de unión al objetivo utilizando PASS Online, Protox-3, SwissADME y análisis de acoplamiento molecular.

Resultados: Se identificaron dieciocho metabolitos por GC-MS y cuarenta y ocho por LC-MS/MS, incluidos luteolina 7-O-glucurónido, baicaleína 6-glucurónido y dihidroresveratrol. Estos compuestos exhibieron actividades antineoplásicas y proapoptóticas previstas favorablemente, así como afinidades de unión estables con los objetivos HER2, caspasa-3 y caspasa-8.

Conclusiones: Esta investigación *in silico* destaca a *M. paleacea* como una fuente prometedora de candidatos contra el cáncer de mama. Estos hallazgos justifican una futura validación *in vitro* e *in vivo* para fundamentar su potencial terapéutico.

Palabras Clave: caspasa; HER2; *Marchantia paleacea*; acoplamiento molecular; descubrimiento de fármacos de productos naturales; perfiles fitoquímicos.

ARTICLE INFO
Received: July 24, 2025.
Accepted: December 9, 2025.
Available Online: January 31, 2026.

AUTHOR INFO
ORCID: 0000-0002-9901-903X (ESS) 0009-0003-9249-0448 (HH)
0000-0002-9895-1853 (PCS) 0009-0009-2203-2904 (MRH)
0000-0001-6236-7017 (NP)

INTRODUCTION

Breast cancer remains one of the most prevalent malignancies and a leading cause of cancer-related mortality among women worldwide, accounting for more than 685,000 deaths in 2020 (Mutiah et al., 2024). In Indonesia, approximately 68,858 new cases were reported during the same period, with a particularly high prevalence among elderly women (Karim et al., 2023). Despite advances in diagnostic techniques and targeted therapies, treatment efficacy is often limited by drug resistance, systemic toxicity, and unequal access to advanced medications (Burguin et al., 2021). These challenges highlight the need for safer, more accessible breast cancer agents derived from natural sources.

The development of HER2-targeted therapy has significantly improved patient outcomes in HER2-positive breast cancer; however, mutation-driven resistance and relapse remain major barriers (Pegram & Jackisch, 2023; Von Minckwitz et al., 2019). HER2, a transmembrane tyrosine kinase receptor, plays a crucial role in regulating cell proliferation and differentiation. Its overexpression accelerates tumor progression and correlates with poor prognosis (Wang & Wu, 2023). Meanwhile, caspase-3 and caspase-8 serve as key apoptotic mediators that regulate programmed cell death, and their dysregulation contributes to cancer cell survival and therapeutic resistance (Kuhlmann et al., 2019; Pu et al., 2017; Zhu et al., 2014). These molecular targets are therefore of interest in identifying new compounds capable of restoring apoptotic signaling and suppressing tumor growth.

Natural products have historically contributed to the discovery of anticancer drugs, providing structurally diverse bioactive compounds with high pharmacological potential (Purkon et al., 2022). Liverworts (*Marchantiophyta*) represent an underexplored group of bryophytes that contain secondary metabolites, such as flavonoids, terpenoids, and bis-bibenzyl derivatives, with antioxidant, antimicrobial, and antiproliferative properties (Purkon et al., 2022). Within this group, the genus *Marchantia* has shown notable biological potential. Previous reports have highlighted its antibacterial, antifungal, and cytotoxic effects, suggesting its potential role in cancer modulation (Siregar et al., 2021).

A representative species of this genus, *Marchantia paleacea* Bertol. (family *Marchantiaceae)*, is distributed in humid, shaded environments and has been used traditionally in parts of Asia for wound healing and liver protection. Recent studies suggest that *Marchantia* species produce bioactive compounds capable of modulating oxidative stress and apoptotic pathways (Purkon et al., 2022). However, comprehensive studies exploring the phytochemical profile of *M. paleacea* and its molecular interactions with key breast cancer targets, such as HER2 and caspases, remain scarce. This gap limits current understanding of its therapeutic value and potential oncology applications.

Therefore, this study aimed to identify and prioritize potential bioactive metabolites from *M. paleacea* using GC–MS and LC–MS/MS analyses, integrated with *in silico* predictions of their biological activity, drug-likeness, and molecular interactions with HER2, caspase-3, and caspase-8. The findings are expected to provide scientific evidence supporting the potential of *M. paleacea* as a natural source of breast anticancer candidates and a foundation for subsequent in vitro and in vivo validation studies.

MATERIAL AND METHODS

Plant collection and extraction

Marchantia paleacea specimens were collected from the roadside area of Panatapan-Berastagi in Karo Regency, North Sumatra, Indonesia (N 03°14′42″ and E 98°32′03,7″). The plant material was identified and authenticated at the Herbarium Medanense (2121/MEDA/2024) of the Department of Biology, Universitas Sumatera Utara. Fresh samples were washed, shade-dried, and ground into fine powder. One kilogram of the powdered material was macerated with 5 L of 70% methanol (HPLC grade; Merck, Germany) for 3 × 24 h under continuous agitation. The extract was filtered through Whatman No. 42 paper (GE Healthcare, UK), centrifuged at 4000 rpm, and concentrated using a rotary evaporator at 40°C under a vacuum pressure of 13.5 kgf/cm². The maceration and concentration processes yielded 500 g of semisolid crude extract from 5 kg of dried plant material, corresponding to an extraction yield of 10% (w/w) (Siregar et al., 2021).

GC-MS analysis

Phytochemical profiling was performed using gas chromatography–mass spectrometry (Bruker GC/MS #1, Japan) on a Bruker Scion TQ/SQ system with helium as the carrier gas. The sample was dissolved in absolute methanol (Sigma-Aldrich, USA) and injected into the gas chromatography-mass spectrometry (GC-MS) system (1 µL injection volume). The analysis was conducted using a FactorFour VF-5ms capillary column (Agilent J&W GC Columns, USA) with 30 m × 0.25 mm i.d. and a 0.25 µm film thickness. The oven temperature was initially set to 50°C for 5 minutes, then increased at 10°C min^{-1} to 280°C and maintained for 15 minutes. The injector temperature was set at

290°C, and the ion source was maintained at 230°C. Peak identification was performed by comparing the obtained mass spectra with reference data (Benet et al., 2016; Mwangi et al., 2024).

LC-MS/MS analysis

Metabolite profiling was conducted using LC-MS/MS (Xevo G2-XS, United Kingdom) with a quadrupole time-of-flight (QToF) mass analyzer (conducted at Saraswanti Indo Genetech, Bogor, Indonesia). Methanolic extracts were diluted and injected (10 µL) into a UPLC-MS (Water Acquity UPLC, USA) system equipped with a Phenomenex Synergi 2.5 µm Fusion-RP 100A (50 × 2.0 mm) column. MS/MS analysis was performed under positive electrospray ionization (ESI) mode, while spectra were acquired in both positive and negative modes using information-dependent acquisition. Desolvation and source temperatures were maintained at 550°C and 120°C, respectively (Alallam et al., 2025; Ali et al., 2021). Compounds were identified based on their retention times, mass-to-charge ratios (m/z), and spectral data following the certified laboratory protocol 18-16-2/MU/SMM-SIG.

Ligand and target protein selection

Three bioactive compounds identified from LC-MS/MS (luteolin 7-O-glucuronide, baicalein 6-glucuronide, and dihydroresveratrol) and the reference drug (lapatinib) were retrieved from the PubChem database (https://pubchem.ncbi.nlm.nih.gov/) in 3D structure format. Target proteins associated with breast cancer were obtained from the Protein Data Bank (https://www.rcsb.org/): HER2 (PDB ID: 3PP0), caspase-3 (PDB ID: 1GFW), and caspase-8 (PDB ID: 1QTN). Protein structures were prepared using BIOVIA Discovery Studio v22.1.100, including the removal of heteroatoms and water molecules.

Prediction of biological activity

The biological activities of the identified metabolites were predicted using the PASS Online web server (http://www.pharmaexpert.ru/passonline/) to estimate the probability of activity (Pa) and the probability of inactivity (Pi). Compounds with Pa > Pi were considered to possess potential biological activity. The analysis focused on pharmacological functions related to anticancer, antioxidant, and anti-inflammatory effects, which were relevant to the study objective. The obtained data were tabulated to highlight the metabolites with the highest predicted anticancer potential (Lagunin et al., 2000).

Toxicity and drug-likeness evaluation

Toxicity profiles were evaluated using the Protox-3 web server (https://tox-new.charite.de/protox_II/) to predict LD_{50} values and corresponding toxicity classes, including hepatotoxicity, carcinogenicity, and immunotoxicity. Drug-likeness and pharmacokinetic properties were analyzed using SwissADME (http://www.swissadme.ch/) based on Lipinski's Rule of Five criteria (molecular weight ≤ 500 Da, LogP ≤ 5, hydrogen bond donors ≤ 5, and hydrogen bond acceptors ≤ 10) (Banerjee et al., 2018). All data were summarized in tables to provide a comprehensive overview of the pharmacokinetics, feasibility, and toxicity of the candidate compound and reference drugs.

Molecular docking

Molecular docking simulations were conducted using PyRx 1.1 integrated with the AutoDock Vina engine to evaluate ligand–protein binding affinities and molecular interactions. The three-dimensional structures of HER2, caspase-3, and caspase-8 were retrieved from the RCSB Protein Data Bank (https://www.rcsb.org/) and prepared by removing water molecules and non-essential heteroatoms. Ligands were energy-minimized and converted into PDBQT format before docking into the defined active site grid boxes of each protein. Validation of the docking protocol was performed by redocking reference ligands, including 03Q (HER2), z-DEVD-FMK (caspase-3), and z-IETD-FMK (caspase-8), under identical docking conditions. The obtained RMSD values (<2.0 Å) confirmed the reliability and reproducibility of the docking procedure. Binding affinities (ΔG, kcal/mol) were used to rank the ligands, and protein–ligand interactions were visualized in PyMOL and Discovery Studio Visualizer, with a focus on hydrogen bonding, hydrophobic contacts, and π–π stacking. The results of *M. paleacea* metabolites were compared with the native and reference ligands to evaluate potential binding similarities and competitive interactions. Docking scores, hydrogen bond residues, and key interaction types were presented in tables and figures, emphasizing the ligands with the strongest predicted anticancer.

RESULTS

GC-MS analysis of *M. paleacea* methanolic extract

GC-MS profiling of the methanolic extract of *M. paleacea* was conducted, revealing 18 distinct chemical constituents identified through comparison of their retention times and relative peak areas (Table 1). Among these, dodecanoic acid, tetradecanoic acid, and n-hexadecanoic acid were detected as the predominant compounds, corresponding to the highest peak intensities.

Dodecanoic acid was identified as the most abundant constituent, with a peak area of 38.1% at a retention time of 18.652 minutes, followed by tetradecanoic acid (21.23%, 21.373 minutes) and n-hexadecanoic acid (10.41%, 22.433 minutes).

Other compounds detected in notable abundance included n-decanoic acid, fatty acid methyl esters, and 1,2-ethanediol. The presence of these constituents reflects a chemically diverse profile comprising alcohols, fatty acids, esters, and hydrocarbons. The repeated detection of dodecanoic acid at different retention times may indicate the presence of structural isomers or fragmentation patterns influenced by ionization conditions.

Several of the identified fatty acids, including tetradecanoic acid (myristic acid), palmitic acid (n-hexadecanoic acid), and lauric acid (dodecanoic acid), have been widely reported for their antimicrobial, anti-inflammatory, and anticancer activities. Although detected in low abundance, thymol represents a compound of particular pharmacological interest due to its established chemopreventive, antibacterial, antifungal, and anti-estrogenic effects (Nagoor Meeran et al., 2017).

Previous studies have further associated these fatty acids with anticancer mechanisms. Dodecanoic acid has been shown to induce apoptosis in breast cancer cells through mitochondrial signaling pathways (Lappano et al., 2017), while n-hexadecanoic acid exhibits anti-inflammatory and pro-apoptotic properties relevant to tumor suppression (Bharath et al., 2021). The identification of these bioactive lipophilic compounds in *M. paleacea* is consistent with earlier reports on other *Marchantia* species containing hexadecanoate and methyl hexadecanoate esters (Purkon et al., 2022). Overall, the GC–MS analysis indicates that *M. paleacea* possesses lipid-based bioactive constituents with significant pharmacological potential, particularly in cancer chemoprevention.

LC-MS/MS analysis

LC-MS/MS-QTOF was utilized for the untargeted screening and identification of *M. paleacea*. The metabolite profile in Table 2 shows that M. paleacea comprises 48 compounds, grouped into distinct chemical classes. In LC-MS/MS analysis, 32 negative ion compounds and 16 positive ion compounds were identified in *M. paleacea*. The LC–MS/MS profiling of the methanolic fraction revealed the presence of approximately seven major metabolites, predominantly belonging to the flavonoid class.

Table 1. GC-MS analysis of *M. paleacea* methanolic extract.

No	RT	Peak name	Peak area (%)	R.Match
1	1.399	1,2-Ethanediol	1.78	745
2	15.003	2,4-Hexadiene	3.85	596
3	15.193	Thymol	0.50	898
4	15.779	1-Undecanol	1.01	776
5	17.731	n-Tridecan-1-ol	1.55	806
6	17.908	Pentadecane	1.52	883
7	18.652	Dodecanoic acid	38.1	848
8	19.921	(Z)-9-Tetradecen-1-ol	0.48	653
9	20.028	(Z)-11-Hexadecen-1-ol	0.49	866
10	20.157	1-Tridecene	0.57	834
11	20.452	2-Dodecanone	0.41	762
12	21.373	Tetradecanoic acid	21.23	864
13	22.433	n-Hexadecanoic acid	10.41	596
14	22.664	3,7-Dimethyl-1,6-octadien-3-ol	0.54	576
15	23.040	Methyl hexadecanoate	2.85	632
16	24.105	n-Decanoic acid	7.94	739
17	26.155	Bicyclo[2.2.1]hept-5-en-2-ol	0.04	519
18	26.391	2-Nitrocyclohexanone	0.09	545

Table 2. LC-MS/MS analysis of *M. paleacea* methanolic extract.

No.	Component name	Formula	Fragments	Isotope match Mz RMS PPM	Retention time (min)	Observed Mass (m/z)	Mass error (ppm)	Adducts
1	p-Tolualdehyde	$C_7H_6O_2$	1	3.34	4.96	121.02923	-3.41	H^-
2	(-)-Epiafzelechin-3-O-β-D-allopyranoside	$C_{21}H_{24}O_{10}$	6	1.07	11.38	435.1286	-1.03	H^-
3	Dihydroresveratrol	$C_{14}H_{14}O_3$	4	2.37	12.83	229.08631	-2.43	H^-
4	2,4,7-Trihydroxy-9,10 dihydrophenanthrene	$C_{14}H_{12}O_3$	1	0.61	11.03	227.0714	0.12	H^-
5	6-Isoinosine	$C_{10}H_{12}N_4O_5$	2	1.08	1.85	267.0734	-0.29	H^-
6	Limocitrin-3-O-β-D-glucopyranoside	$C_{23}H_{24}O_{13}$	8	0.81	10.65	507.11414	-0.54	H^-
7	Resokaempferol	$C_{15}H_{10}O_5$	3	1.50	12.30		-1.39	H^-
8	3,4′,5-Trihydroxy-3′,7 dimethoxyflavanone	$C_{17}H_{16}O_7$	6	2.22	14.19	331.0815	-2.41	H^-
9	(R)-Prechrysophanol	$C_{15}H_{14}O_4$	2	1.71	16.64	257.0818	-0.69	H^-
10	2,4,5 Trihydeoxybenzaldehyde	$C_7H_6O_4$	1	3.88	2.83	153.0187	-3.91	H^-
11	Guaiacol	$C_7H_8O_2$	1	3.92	3.00	123.0447	-3.76	H^-
12	Dendrocandin E	$C_{15}H_{16}O_5$	2	1.38	12.82	275.0921	-1.38	H^-
13	Vanillyl alcohol	$C_8H_{10}O_3$	3	4.60	2.99	153.0550	-1.38	H^-
14	p-Hydroxyphenol	$C_6H_6O_2$	1	3.24	2.83	109.0291	-3.32	H^-
15	Euparin	$C_{13}H_{12}O_3$	2	1.80	8.55	215.0712	-0.63	H^-
16	Flavanthrinin	$C_{15}H_{12}O_3$	2	1.26	15.86	239.0711	1.06	H^-
17	Luteolin-7-O-glucuronide	$C_{21}H_{18}O_{12}$	5	1.60	8.77	461.07288	0.71	H^-
18	Baicalein-6-glucuronide	$C_{21}H_{18}O_{11}$	14	1.15	9.98	445.07737	-0.59	H^-
19	(3R)-4′-Methoxy-2′,3′,7 trihydroxy-isoflavanone	$C1_6H_{14}O_6$	4	2.85	9.76	301.0716	-0.39	H^-
20	Genistein	$C_{15}H_{10}O_5$	4	2.16	11.31	269.0452	-1.11	H^-
21	Kaempferol	$C_{15}H_{10}O_6$	2	0.78	9.90	285.0405	-0.04	H^-
22	5,7-Dihydroxychromone	$C_9H_6O_4$	1	0.66	7.93	177.01942	0.52	H^-
23	Mirificin	$C_{26}H_{28}O_{13}$			8.93	547.1463	0.99	H^-
24	3'-O-Methyltaxifolin	$C_{16}H_{14}O_7$	8	1.34	11.32	317.0663	-1.31	H^-
25	5,7,8,4′-Tetrahydroxy flavone	$C_{15}H_{10}O_6$	1	0.87	8.78	285.0406	0.40	H^-
26	Eriodictyol-7-O-β-D methyl glucuronopyranoside	$C_{22}H_{22}O_{12}$	8	0.41	10.63	477.1037	-0.33	H^-
27	dl-Umtatin	$C_{15}H_{14}O_5$	1	1.66	10.01	273.0772	1.42	H^-
28	(2R,3R)-3,5,7,2′,6′ Pentahydroxy flavanone	$C_{15}H_{12}O_7$	1	1.00	9.59	303.0513	0.79	H^-
29	Pinocembrin_1	$C_{15}H_{12}O_4$	1	1.57	12.22	255.0667	1.52	H^-
30	Gentiatibetine	$C_9H_{11}NO_2$	1	3.31	2.18	164.07111	-3.44	H^-
31	Irilone	$C_{16}H_{10}O_6$	1	2.45	13.47	297.04135	1.42	H^-
32	Leucocyanidin	$C_{15}H_{14}O_7$	4	2.79	9.99	305.0660	-2.34	H^-
33	Daidzin_1	$C_{21}H_{20}O_9$	3	0.19	8.02	23.871	-0.12	H^+
34	Jaceosidin	$C_{17}H_{14}O_7$	2	0.37	15.20	24.945	0.06	H^+
35	5,6,7,3′-Tetrahydroxy-4′-methoxyisoflavone	$C_{16}H_{12}O_7$	1	2.11	10.71	1.145	1.50	H^+
36	Myricetin 3′,5′-dimethyl ether 3-O-β-D-glucopyranoside	$C_{23}H_{24}O_{13}$	9	0.82	10.66	16.525	0.70	H^+
37	(3α,4β,5α)-4,5-Dihydro-4,5-dimethyl-3-(1-pyrrolyl)-furan-2(3H)-one	$C_{10}H_{13}NO_2$	2	3.30	1.26	17.012	3.15	H^+
38	1-Carbomethoxy-β-carboline	$C_{13}H_{10}N2O_2$	1	1.05	9.37	3.751	-0.77	H^+
39	Flavanthrinin	$C_{15}H_{12}O_3$	1	1.57	15.06	55.058	1.59	H^+
40	2-Hydroxy-5-methylhypnone	$C_9H_{10}O_2$	1	2.99	9.94	1.861	2.73	H^+
41	Haematoxylin	$C_{16}H_{14}O_6$	2	1.09	10.64	19.550	1.08	H^+
42	Sulfuretin	$C_{15}H_{10}O_5$	1	1.34	13.83	47.048	1.36	H^+
43	6-Gingerdione	$C_{17}H_{24}O_4$	1	1.07	8.07	1.471	-0.67	H^+
44	1,8-Dihydroxy-2,3,6-trimethoxyxanthone	$C_{16}H_{14}O_7$	1	0.47	11.32	103.299	0.52	H^+
45	Luteolin-7-O-glucuronide	$C_{21}H_{18}O_{12}$	7	1.21	9.91	320.400	1.16	H^+
46	Adenosine	$C_{10}H_{13}N_5O_4$	5	1.93	1.70	157.521	1.91	H^+
47	Baicalein-6-glucuronide	$C_{21}H_{18}O_{11}$	5	0.57	9.98	76.066	0.54	H^+
48	5,7-Dihydroxychromone	$C_9H_6O_4$	1	3.36	7.95	13.719	3.38	H^+

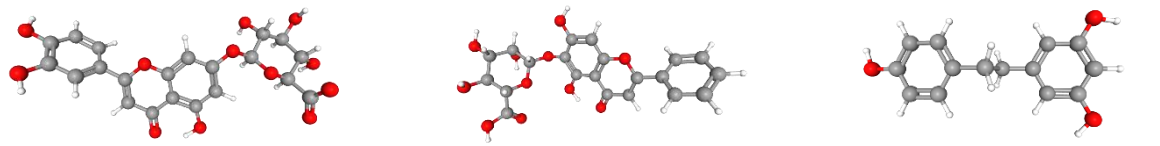


Figure 1. 3D Compound structures from LC-MS/MS analysis of *M. paleacea* extract.
(A) Luteolin-7-O- glucuronide (NCBI, 2025a); **(B)** Baicalein-6-glucuronide (NCBI, 2025b); **(C)** Dihydroresveratrol (NCBI, 2025c).

Table 3. Biological activity prediction of *M. paleacea* phytocompounds

Compound name	Pa score	Pi score	Biological activity
Luteolin-7-O- glucuronide	0.837	0.003	Antioxidant
	0.733	0.012	Apoptosis agonist
	0.432	0.027	Antineoplastic (breast cancer)
	0.417	0.041	Antimetastatic
Baicalein-6-glucuronide	0.817	0.003	Antioxidant
	0.791	0.009	Apoptosis agonist
	0.429	0.038	Antimetastatic
	0.349	0.042	Antineoplastic (breast cancer)
Dihydroresveratrol	0.545	0.033	Apoptosis agonist
	0.374	0.014	Antioxidant
	0.256	0.069	Antineoplastic (breast cancer)

Pa: Probability of activity; Pi: Probability of inactivity.

The key compounds identified included baicalein-6-glucuronide, luteolin-7-O-glucuronide, genistein, kaempferol, and 3′-O-methyltaxifolin. Among them, baicalein-6-glucuronide exhibited the highest ion intensity in the positive ionization mode (H^+), while luteolin-7-O-glucuronide also showed a strong signal, suggesting its considerable abundance in the extract.

Baicalein-6-glucuronide was detected with high intensity under the positive ionization mode, suggesting its considerable abundance in the extract. Luteolin-7-O-glucuronide likewise exhibited a prominent signal under the same conditions. Both compounds are well recognized for their diverse pharmacological activities, particularly in modulating oxidative stress and inhibiting cancer progression. The chemical structures of these key flavonoids are presented in Fig. 1.

Predicted bioactivity of *M. paleacea* compounds

The LC-MS/MS analysis identified three compounds for molecular docking analysis: Luteolin 7-O-glucuronide, baicalein 6-glucuronide, and dihydroresveratrol. The compounds were among the most prevalent metabolites detected in the methanol extract of *M. paleacea*. All three compounds demonstrated anticipated anticancer and anti-inflammatory biological activities, making them suitable candidates for further computational analysis. The chemical structures of the chosen compounds were obtained from the PubChem database. The analysis of biological activity was conducted using the Pa and Pi values. A high Pa value indicates a high probability based on structural similarity; however, experimental validation is still required (Pramely & Raj, 2012). The findings indicated that all compounds exhibited diverse activities linked to anticancer potential, encompassing antioxidant, apoptosis-inducing, antineoplastic, and anti-metastatic properties. The Pa scores for each compound, presented in Table 3, corroborated these results.

ADMET drug-likeness analysis

Toxicity evaluation provides an important indication of a compound's safety profile and helps determine whether its biological activity can be pursued for therapeutic development. As shown in Table 4, all *M. paleacea* metabolites were predicted to belong to toxicity class 5, corresponding to LD_{50} values around 5000 mg/kg, which suggests a very low level of acute toxicity. Both luteolin-7-O-glucuronide, baicalein-6-glucuronide, and dihydroresveratrol were classified as

non-hepatotoxic and non-cytotoxic, with high probabilities (> 0.75) for the inactive category. In contrast, the control and reference compounds—lapatinib, z-DEVD-FMK, and z-IETD-FMK—showed relatively higher predicted toxicity (classes 3–4), indicating that the phytoconstituents may provide a wider safety margin than conventional anticancer agents. This favorable toxicity profile supports the therapeutic relevance of *M. paleacea* metabolites in breast cancer treatment, particularly given their predicted safety, which aligns with the low cytotoxicity often observed in plant-derived compounds with selective anticancer mechanisms. The absence of hepatotoxicity is particularly encouraging, as hepatotoxicity remains a major limitation of many synthetic chemotherapeutics. Together, these *in silico* findings from Protox-3 and SwissADME suggest that the identified compounds possess promising safety profiles and are suitable for further exploration as potential breast anticancer candidates, although experimental validation remains essential to confirm these predictions.

The evaluation of drug-likeness using Lipinski's Rule of Five provides an essential early-stage assessment of a compound's suitability for oral drug development (Benet et al., 2016). As presented in Table 5, both luteolin-7-O-glucuronide and baicalein-6-glucuronide exhibited two violations, exceeding the acceptable limits for hydrogen bond donors and acceptors. These deviations arise from the presence of multiple hydroxyl and glucuronic acid groups, which increase molecular polarity and hydrogen-bonding potential. Although such structural features enhance aqueous solubility and molecular recognition, they concurrently reduce passive membrane permeability, limiting the likelihood of efficient gastrointestinal absorption. This observation is consistent with the known pharmacokinetic behavior of glucuronide conjugates, which often function as metabolic derivatives with low oral bioavailability but may regain activity *in vivo* through enzymatic hydrolysis to their parent aglycones. In contrast, dihydroresveratrol, which met all Lipinski parameters, exhibited optimal physicochemical properties, suggesting improved permeability and absorption potential. The reference drug lapatinib, despite one violation due to its molecular weight, remains an orally active HER2 inhibitor, illustrating that Lipinski's rules serve as guiding principles rather than absolute barriers. Meanwhile, the peptide-based caspase inhibitors z-DEVD-FMK and z-IETD-FMK each showed two violations, reflecting their high molecular weight and poor oral absorption, consistent with their experimental rather than clinical use.

Table 4. ADMET analysis of the *M. paleacea* phytocompounds

Compound	Toxicity class	LD_{50} (mg/kg)	Accuracy (%)	Probability	
				Hepatotoxicity	Cytotoxicity
Luteolin7-O- glucuronide	5	5000	69.26%	0.75 (Inactive)	0.91 (Inactive)
Baicalein-6-glucuronide	5	5000	69.26%	0.75 (Inactive)	0.91 (Inactive)
Dihydroresveratrol	5	2450	69.26%	0.77 (Inactive)	0.93 (Inactive)
Lapatinib	4	1500	23%	0.90 (Active)	0.76 (Active)
z-DEVD-FMK	4	920	67.38	0.84 (Inactive)	0.65 (Inactive)
z-IETD-FMK	3	300	67.38	0.84 (Inactive)	0.69 (Inactive)

Table 5. Drug-likeness prediction of the *M. paleacea* phytocompounds.

Compound	Lipinski's Rule of Five				Violation
	Molecular weight (≤ 500 g/mol)	Hydrogen donor (≤ 5)	Hydrogen acceptor (≤ 10)	LogP (<5)	
Luteolin7-O- glucuronide	462.36	7	12	-2.12	2
Baicalein-6-glucuronide	446.36	6	11	-1.63	2
Dihydroresveratrol	230.26	3	3	2.34	0
Lapatinib	581.06	2	8	4.20	1
z-DEVD-FMK	668.66	4	13	1.34	2
z-IETD-FMK	654.68	5	12	1.37	2

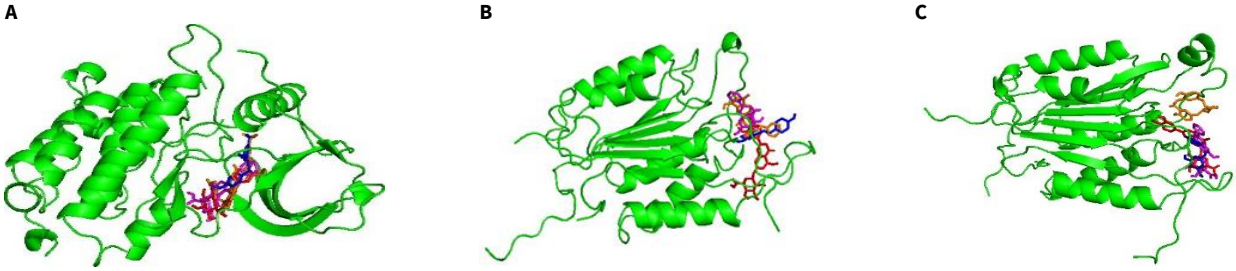


Figure 2. 3D Visualization of protein, ligand complexes, and top three compounds.

(A) HER2 protein complex (green) with luteolin 7-O-glucuronide (red), baicalein-6-glucuronide (magenta), dihydroresveratrol (blue), and O3Q (orange); **(B)** Caspase 3 protein complex (green) with luteolin 7-O-glucuronide (red), baicalein-6-glucuronide (magenta), dihydroresveratrol (blue), and MSI (orange); **(C)** Caspase 8 protein complex (green) with luteolin 7-O-glucuronide (red), baicalein-6-glucuronide (magenta), dihydroresveratrol (blue), and rosmarinic acid (orange).

These findings suggest that while the glucuronidated flavonoids of *M. paleacea* exhibit promising bioactivity, their limited permeability warrants consideration of advanced formulation strategies—such as prodrug modification, nano-encapsulation, or tumor-targeted delivery systems—to enhance bioavailability and therapeutic efficacy (Vazhappilly et al., 2021).

Luteolin is a widely distributed flavonoid found in numerous plant families and is well known for its broad pharmacological potential. Plants rich in luteolin have long been used in traditional medicine to manage various diseases, including cancer (Mahwish et al., 2025). Recent evidence by Velmurugan et al. (2020) demonstrated that luteolin-7-O-glucoside effectively suppresses oral cancer cell metastasis by inhibiting the p38 MAPK signaling pathway and downregulating MMP-2 expression. Furthermore, Caporali et al. (2022) reported that luteolin sustains the phosphorylated state of STAT1 within the JAK/STAT and Wnt/β-catenin signaling axes by inhibiting SHP-2 phosphatase activity, thereby enhancing STAT1-mediated signaling and attenuating cancer cell proliferation. Similarly, baicalein-6-glucuronide and dihydroresveratrol are recognized as derivative polyphenolic compounds with notable anticancer potential. Hu et al. (2022) demonstrated that baicalein suppresses epithelial–mesenchymal transition (EMT) by downregulating TGF-β signaling via inhibition of the NF-κB pathway in breast epithelial cells. In addition, Morshed et al. (2023) showed that baicalein inhibits the Wnt/β-catenin pathway, thereby limiting breast cancer metastasis by suppressing EMT. Furthermore, these findings underscore the therapeutic relevance of these flavonoid and stilbene derivatives as multitargeted modulators of cancer-associated signaling pathways.

Molecular docking analysis

The compounds identified by LC-MS/MS were correlated with antioxidant and anticancer activities and were subjected to molecular docking at the HER2, caspase 3, and caspase 8 target sites. Molecular docking validation was conducted to ensure that the process closely reflected the physiological conditions in the human body. The interaction between the compounds of interest and the control with the HER2 protein (PDB ID 3PP0) as well as the native ligand, 2-(2-[4-((5-chloro-6-[3-(trifluoromethyl)phenoxy] pyridin-3-yl)amino)-5H-pyrrolo[3,2 d]pyrimidin-5 yl]ethoxy)ethanol (03Q), which served as a template to determine the location of the active site, was examined Fig. 2. These results showed that luteolin 7-O-glucuronide and baicalein-6-glucuronide had a relatively negative binding affinity (Table 6). The binding affinity scores of these compounds were compared to the control (03Q), with results showing that luteolin 7-O-glucuronide and baicalein-6-glucuronide exhibited binding affinities of -10.7 kcal/mol and -10.2 kcal/mol, respectively. However, these scores were not as negative as the control, which had a binding affinity of -11.1 kcal/mol.

The interaction between the compounds of interest and the control with caspase 3 (PDB ID 1GFW) and the native ligand, 1-methyl-5-(2-phenoxymethyl-pyrrolidine-1-sulfonyl)-1H-indole-2,3-dione (MSI), showed that luteolin 7-O-glucuronide, baicalein-6-glucuronide, and dihydroresveratrol had binding affinities approaching that of the control, with values of -8.4 kcal/mol, -7.8 kcal/mol, and -7.1 kcal/mol, respectively. These scores were not sufficiently negative, as shown by the control's binding affinity score of -9.1 kcal/mol. The interaction of the compounds of interest with caspase 8 (PDB ID 1QTN) and the native ligand, rosmarinic acid, showed that luteolin 7-O-glucuronide and baicalein-6-glucuronide had more negative binding affinities compared to the control, with values of -8.8 kcal/mol and -8.3 kcal/mol, while the control had a value of -6.4 kcal/mol.

Table 6. Binding affinity for the selected compounds of the *M. paleacea* and breast cancer-related proteins.

Protein	Compound	Binding affinity score (Kcal/mol)	Exhaustiveness	Grid position
HER2	03Q (Control)	-11.1	8	X = 17.735
	Luteolin 7-O-glucuronide	-10.7	8	Y = 13.912
	Baicalein-6-glucuronide	-10.2	8	Z = 28.534
	Dihydroresveratrol	-9.1	8	
Caspase 3	MSI (Control)	-9.1	8	X = 37.881
	Luteolin 7-O-glucuronide	-8.4	8	Y = 28.552
	Baicalein-6-glucuronide	-7.8	8	Z = 25.499
	Dihydroresveratrol	-7.1	8	
Caspase 8	Rosmarinic acid (control)	-6.4	8	X = -10.855
	Luteolin 7-O-glucuronide	-8.8	8	Y = 32.645
	Baicalein-6-glucuronide	-8.3	8	Z = 42.689
	Dihydroresveratrol	-6.0	8	

The results of molecular docking analysis presented in Table 6 demonstrate that several compounds from *M. paleacea*, including luteolin-7-O-glucuronide and baicalein-6-glucuronide, show strong binding affinity against breast cancer-related targets such as HER2, CASP8, and CASP3. These values were qualitatively compared with reported docking scores for standard drugs such as tamoxifen and trastuzumab (−9.4 kcal/mol for HER2), as documented in previous studies (Ávila-Gálvez et al., 2020; Hardianto et al., 2023). Several ligands in our dataset showed comparable or stronger interactions, suggesting potential for further pharmacological investigation.

Docking studies show that luteolin 7-O-glucuronide interacts with HER2 through the formation of hydrogen bonds with GLY A:804, pi-alkyl interaction with ALA A:751, and van der Waals interactions with ARG A:849, GLY A:727, LEU A:807, ASP A:808, LEU A:800, GLN A:799, ASP A:863, THR A:798, VAL A:797, LEU A:796, LEU A:785, ILE A:752, THR A:862, GLY A:729, ALA A:730, and ASN A:850 (Fig. 3). Baicalein 6-glucuronide interacts with HER2 by forming hydrogen bonds with amino acid residues such as SER A:728 and CYS A:805. Meanwhile, the interaction of dihydroresveratrol with HER2 shows hydrogen, alkyl, and van der Waals bonds (Fig. 3).

The 2D interaction between luteolin 7-O-glucuronide and caspase 3 showed the formation of hydrogen bonds with TRP B:214, GLN B:217, and PHE B:250, as well as a pi-cation bond with ARG B:207. As shown in Fig. 4, the interaction of baicalein 6-glucuronide with CAS3 showed the formation of hydrogen bonds with SER A:65, SER A:63, ARG B:207, SER B:209, SER B:205, CYS A:163, and THR A:62. In addition, covalent and van der Waals bonds were also observed in this interaction. CAS3-dihydroresveratrol formed van der Waals bonds with ASP B:253, SER B:215, TYR B:204, CYS A:163, SER B:205, and ARG B:207. The interaction of protein caspase 8 with the compounds of interest was further analyzed to identify the amino acid residues in the complex.

These results showed that various types of bonds were present at the active site of the protein. The same amino acid residues found in the binding of the control and the compounds of interest showed that CAS8-luteolin 7-O-glucuronide, CAS8-baicalein 6-glucuronide, and CAS8-dihydroresveratrol had van der Waals and hydrogen bonds. In addition, the amino acid residues involved in the binding of luteolin 7-O-glucuronide, baicalein 6-glucuronide, and dihydroresveratrol to CAS8 provided important information that these compounds bind with good affinity and require lower concentrations to reduce CAS8 activity (Fig. 5).

Dihydroresveratrol emerged as the negative ion compound that demonstrated favorable properties in accordance with Lipinski's rules, exhibiting effective interactions with the target proteins. Furthermore, it exhibited hydrogen bond interactions with the HER2 protein at residue SER A:783 and van der Waals interactions with the CAS3 protein, specifically at residues ASP B:253, SER B:215, TYR B:204, CYS A:163, SER B:205, and ARG B:207. Dihydroresveratrol exhibited hydrogen bonds and van der Waals interactions with the CAS8 protein. The amino acid residues in luteolin 7-O-glucuronide and baicalein 6-glucuronide demonstrate significant interactions with the target protein, indicating a high binding affinity for these compounds. Furthermore, favorable binding interactions were observed, suggesting that the

compounds may exert inhibitory effects on the target protein even at low concentrations. *M. paleacea* exhibits potential as a candidate for anticancer drug development, especially in the context of breast cancer treatment. This study identified active compounds in *M. paleacea,* revealing that three dominant compounds—luteolin 7-O-glucuronide, baicalein 6-glucuronide, and dihydroresveratrol—exhibit potential as anticancer agents for breast cancer therapy.

Binding affinity values, expressed in kcal/mol, indicate the strength of interaction between a compound and its target protein, with lower (more negative) values corresponding to stronger binding. As shown in Table 7, all control ligands displayed stable and meaningful interactions with their respective targets, supporting the reliability of the docking protocol. Lapatinib (PubChem CID: 208908), the reference inhibitor of HER2, exhibited a binding affinity of −7.8 kcal/mol with an RMSD of 1.686 Å, suggesting a well-fitted pose within the active site. This result aligns with lapatinib's established role as a potent HER2 tyrosine kinase inhibitor used clinically in breast cancer therapy. For the apoptotic targets, z-DEVD-FMK (CID: 16760394) and z-IETD-FMK (CID: 25108681) demonstrated strong binding affinities of −7.4 kcal/mol and −8.1 kcal/mol, respectively, with RMSD values ≤ 2.0 Å, confirming accurate and reproducible docking results.

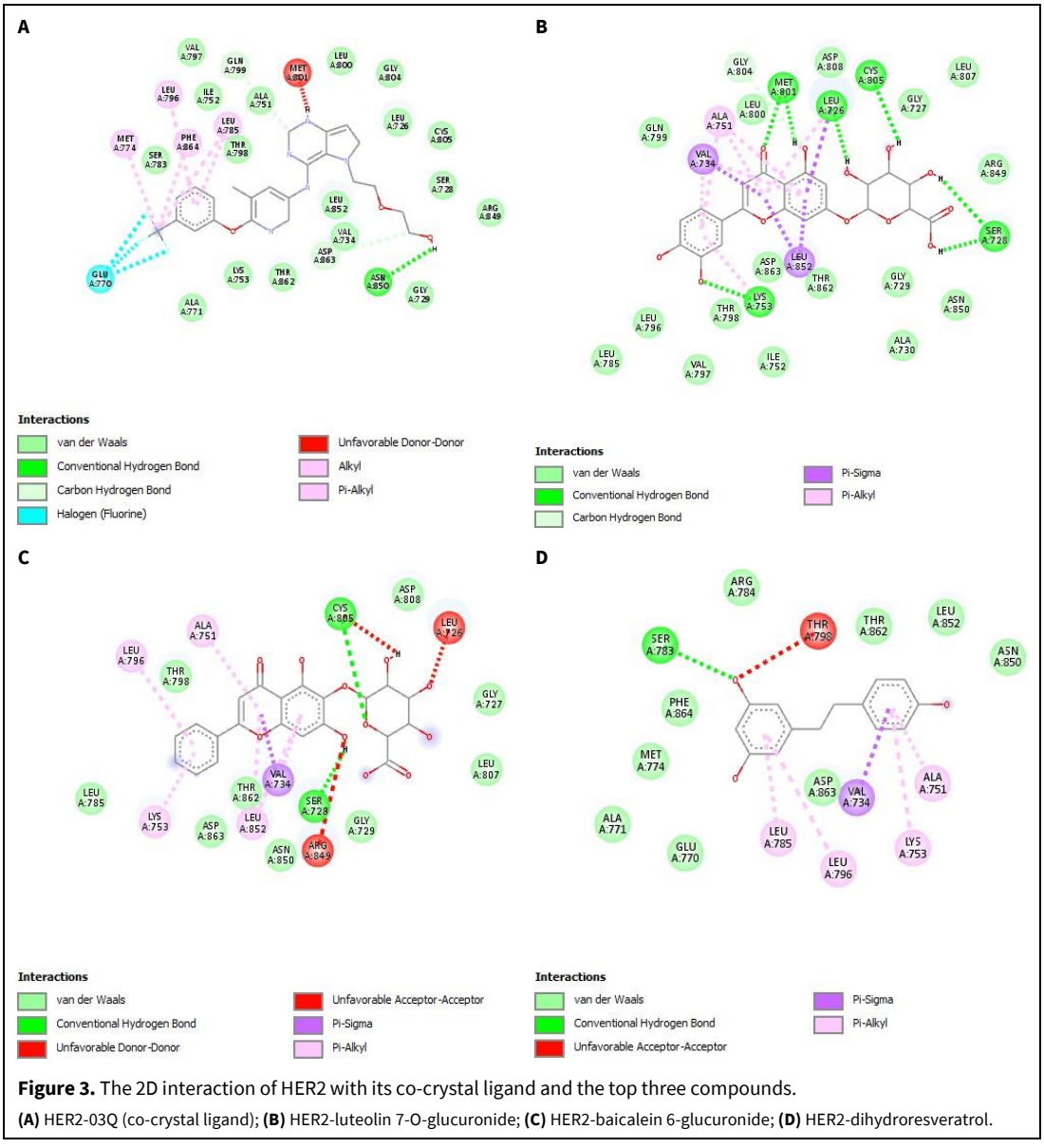


Figure 3. The 2D interaction of HER2 with its co-crystal ligand and the top three compounds.
(A) HER2-03Q (co-crystal ligand); **(B)** HER2-luteolin 7-O-glucuronide; **(C)** HER2-baicalein 6-glucuronide; **(D)** HER2-dihydroresveratrol.

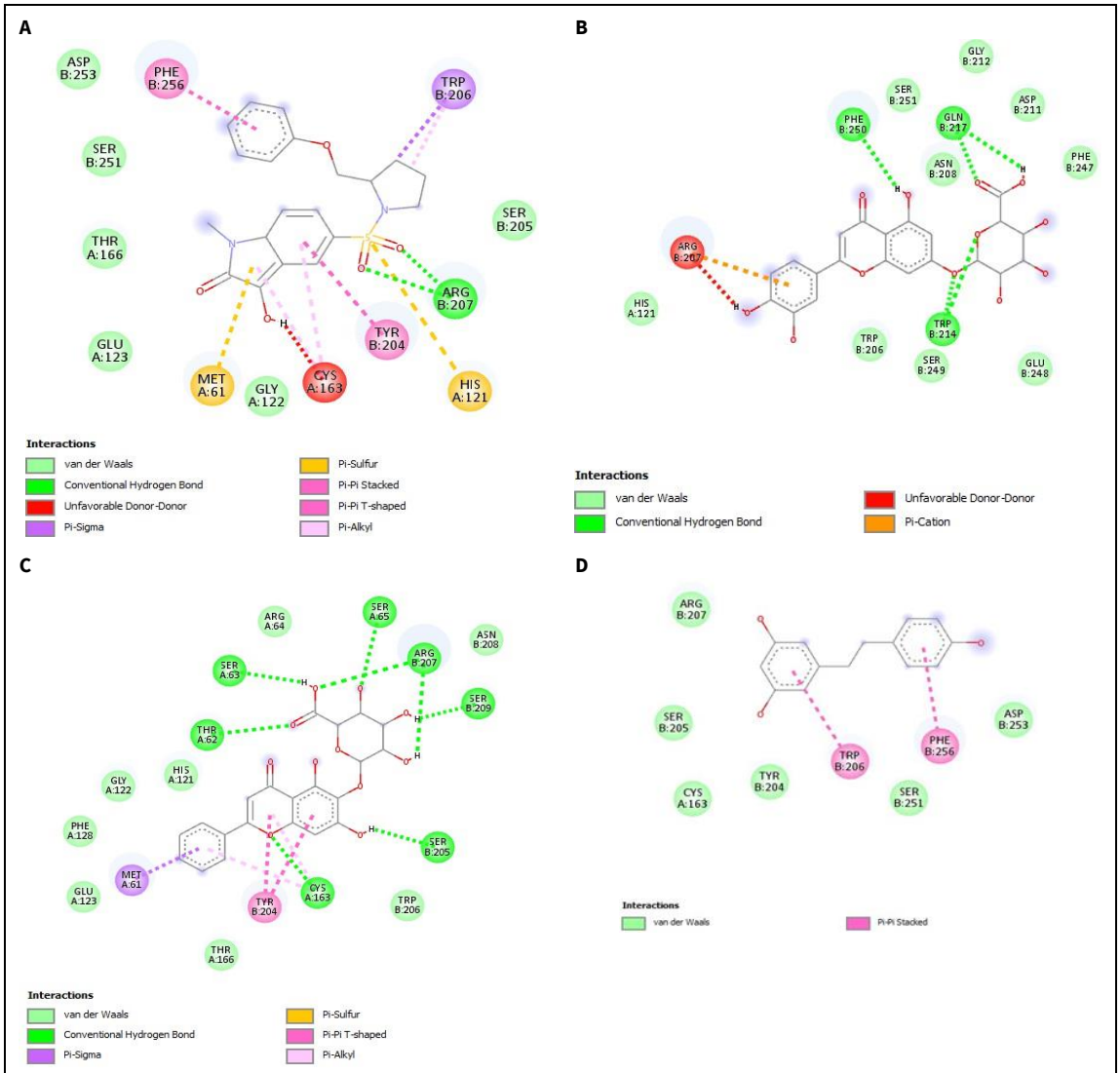


Figure 4. The 2D interaction of CASP-3 and the top three compounds.
(A) CAS3-MSI (control); **(B)** CAS3-luteolin 7-O-glucuronide; **(C)** CAS3-baicalein 6-glucuronide; **(D)** CAS3-dihydroresveratrol.

Notably, z-IETD-FMK exhibited the most favorable binding energy, reflecting its strong interaction with the caspase-8 active site and its reported irreversible inhibition of apoptosis. Furthermore, these validation results confirm that the docking setup and grid parameters accurately reproduced biologically relevant ligand–protein interactions, ensuring the reliability of the computational framework used to evaluate the *M. paleacea* metabolites in subsequent docking analyses.

DISCUSSION

Several bioactive metabolites identified in *M. paleacea* exhibit mechanisms consistent with established anticancer pathways. Luteolin-7-O-glucuronide has been reported to suppress metastasis in oral and breast cancer by downregulating MMP-2 and modulating the p38 MAPK and Wnt/β-catenin signaling pathways (Caporali et al., 2022; Velmurugan et al., 2020). Similarly, baicalein-6-glucuronide exerts antitumor effects by inhibiting epithelial–mesenchymal transition and NF-κB signaling, thereby limiting breast cancer cell migration and invasion (Hu et al., 2022; Morshed et al., 2023). Dihydroresveratrol, a metabolite of resveratrol, exhibits anti-inflammatory and antiproliferative activity by modulating apoptotic gene expression and disrupting mitochondrial membrane potential (Cotino-Nájera et al., 2023; Simanullang et al., 2022).

Fatty acids detected through GC–MS, such as tetradecanoic acid and n-hexadecanoic acid (palmitic acid), are known to induce apoptosis and endoplasmic reticulum stress in various cancer models, while dodecanoic acid (lauric acid) triggers mitochondrial-dependent apoptotic signaling in breast cancer cells (Bharath et al., 2021; Lappano et al., 2017).

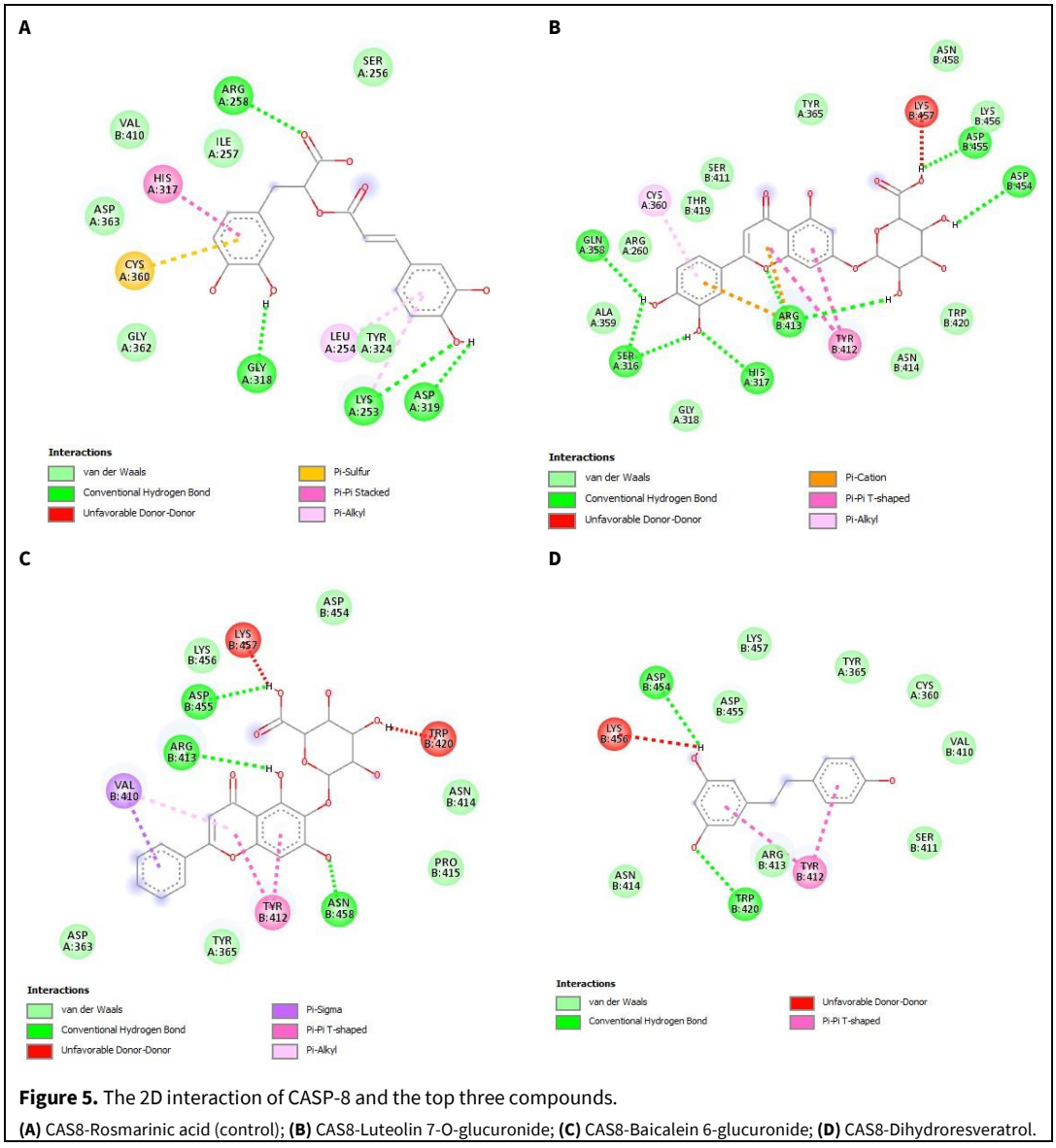


Figure 5. The 2D interaction of CASP-8 and the top three compounds.
(A) CAS8-Rosmarinic acid (control); **(B)** CAS8-Luteolin 7-O-glucuronide; **(C)** CAS8-Baicalein 6-glucuronide; **(D)** CAS8-Dihydroresveratrol.

Table 7. Validation of HER2, caspase 3, and caspase 8 with their pharmacological ligands.

Target protein	Compound	Binding affinity Dcore (kcal/mol)	RMSD	Grid box (x;y;z)
HER2	Lapatinib	-7.8	1.686	23.7500;29.5655;-1.3538
Caspase-3	z-DEVD-FMK	-7.4	≤2.0 Å	20.7951;30.3364;14.5859
Caspase-8	z-IETD-FMK	-8.1	≤2.0 Å	-9.2706;32.1198;43.0689

Thymol, also identified in the extract, has been described as an aromatase inhibitor capable of downregulating estrogen receptor signaling in hormone-responsive breast cancer (Nagoor Meeran et al., 2017). Collectively, these structure–activity insights support the predicted bioactivities of *M. paleacea* metabolites and highlight their potential relevance in breast cancer pharmacology.

In silico predictions further supported these findings. The PASS Online results indicated strong anticancer-related activities, while molecular docking showed that luteolin-7-O-glucuronide, baicalein-6-glucuronide, and dihydroresveratrol demonstrated notable binding affinities for HER2, caspase-3, and caspase-8, in some cases exceeding those of reference drugs (Situmorang et al., 2025a; 2025b). Benchmarking with its pharmacological ligands yielded RMSD values ≤ 2.0 Å, confirming the reliability of the docking. Residue-level interaction analyses revealed that these compounds formed stable hydrogen bonds and hydrophobic contacts within the receptor active sites, supporting their predicted pharmacological potential.

Despite these promising computational insights, the results were interpreted as hypothesis-generating rather than confirmatory. The study is limited by the absence of experimental validation, and all toxicity and activity predictions remain computational. Therefore, future investigations should incorporate *in vitro* assays such as MTT cytotoxicity testing, Annexin V/PI staining, and Western blotting for apoptotic markers (caspase-3, Bcl-2, Bax) to confirm predicted mechanisms. *In vivo* studies using breast cancer xenograft models are also necessary to evaluate therapeutic efficacy, pharmacokinetics, and safety in biological systems.

In conclusion, this study provides a preliminary *in silico* and phytochemical foundation for understanding the breast anticancer potential of *M. paleacea* metabolites. The findings highlight luteolin-7-O-glucuronide, baicalein-6-glucuronide, and dihydroresveratrol as promising leads for further pharmacological evaluation, offering a rational starting point for targeted *in vitro* and *in vivo* exploration of their roles in breast cancer therapy.

CONCLUSION

This study identified key bioactive metabolites from *M. paleacea,* including luteolin 7-O-glucuronide, baicalein 6-glucuronide, and dihydroresveratrol, through integrated GC-MS, LC-MS/MS, and molecular docking analyses, indicating their potential as breast cancer therapy candidates. These compounds exhibited strong predicted binding affinities for HER2, caspase-3, and caspase-8, along with favorable toxicity and drug-likeness profiles. While the computational outcomes highlight promising pharmacological potential, they primarily establish a framework for prioritizing experimental validation. Further *in vitro* and *in vivo* studies are essential to substantiate their therapeutic efficacy and clarify underlying molecular mechanisms in breast cancer models.

CONFLICT OF INTEREST

The research was conducted entirely free from any involvement in commercial, financial, or personal matters that might be perceived as a possible conflict of interest or that could have influenced the outcomes or interpretation of the study.

ACKNOWLEDGMENTS

The authors were grateful to Indonesia's Ministry of Education, Culture, Study, and Technology for funding this study through the "DRPM with contract number: 25/UNS.4.10.S/PPM/KP-DRTPM/2024".

GENERATIVE ARTIFICIAL INTELLIGENCE (AI)

The authors declare that no generative artificial intelligence (AI) or AI-assisted technologies were used in the preparation, writing, or editing of this manuscript. All content was developed solely by the authors, who take full responsibility for its accuracy and integrity.

REFERENCES

Alallam B, Abdulameed HT, Lim V (2025) Unbiased metabolomic and chemometric profiles of three *Sargassum polycystum* extracts using GCMS and LCMS/MS: content analysis, correlation analysis and molecular docking. Food Chem 470: 142666. https://doi.org/10.1016/j.foodchem.2024.142666

Ali A, Bashmil YM, Cottrell JJ, Suleria HAR, Dunshea FR (2021) LC-MS/MS-QTOF screening and identification of phenolic compounds from Australian grown herbs and their antioxidant potential. Antioxidants 10(11): 1770. https://doi.org/10.3390/antiox10111770

Ávila-Gálvez MÁ, Giménez-Bastida JA, Espín JC, González-Sarrías A (2020) Dietary phenolics against breast cancer: A critical evidence-based review and future perspectives. Int J Mol Sci 21(16): 5718. https://doi.org/10.3390/ijms21165718

Banerjee P, Eckert AO, Schrey AK, Preissner R (2018) ProTox-II: A webserver for the prediction of toxicity of chemicals. Nucleic Acids Res 46(W1): W257–W263. https://doi.org/10.1093/nar/gky318

Benet LZ, Hosey CM, Ursu O, Oprea TI (2016) BDDCS, the Rule of 5 and drugability. Adv Drug Deliv Rev 101: 89–98. https://doi.org/10.1016/j.addr.2016.05.007

Bharath B, Perinbam K, Devanesan S, AlSalhi MS, Saravanan M (2021) Evaluation of the anticancer potential of hexadecanoic acid from brown algae *Turbinaria ornata* on HT-29 colon cancer cells. J Mol Struct 1235: 130229. https://doi.org/10.1016/j.molstruc.2021.130229

Burguin A, Diorio C, Durocher F (2021) Breast cancer treatments: Updates and new challenges. J Pers Med 11(8): 808. https://doi.org/10.3390/jpm11080808

Caporali S, Di Stefano A, Calabrese C, Giovannelli A, Pieri M, Savini I, Tesauro M, Bernardini S, Minieri M, Terrinoni A (2022) Anti-inflammatory and active biological properties of the plant-derived bioactive compounds luteolin and luteolin 7-glucoside. Nutrients 14(6): 1155. https://doi.org/10.3390/nu14061155

Cotino-Nájera S, Herrera LA, Domínguez-Gómez G, Díaz-Chávez J (2023) Molecular mechanisms of resveratrol as chemo- and radiosensitizer in cancer. Front Pharmacol 14: 1287505. https://doi.org/10.3389/fphar.2023.1287505

Hardianto A, Mardetia SS, Destiarani W, Budiman YP, Kurnia D, Mayanti T (2023) Unveiling the anti-cancer potential of onoceranoid triterpenes from *Lansium domesticum* Corr. cv. Kokosan: An *in silico* study against estrogen receptor alpha. Int J Mol Sci 24(19): 15033. https://doi.org/10.3390/ijms241915033

Hu Z, Guan Y, Hu W, Xu Z, Ishfaq M (2022) An overview of pharmacological activities of baicalin and its aglycone baicalein: New insights into molecular mechanisms and signaling pathways. Iran J Basic Med Sci 25(1): 14–26. https://doi.org/10.22038/IJBMS.2022.60380.13381

Karim BK, Tsamarah DF, Zahira A, Rosandi NF, Swarga KF, Aulifa DL, Elaine AA, Sitinjak BDP (2023) In-silico study of active compounds in guava leaves (*Psidium guajava* L.) as candidates for breast anticancer drugs. Indones J Biol Pharm 3(3): 194–209. https://doi.org/10.24198/ijbp.v3i3.52060

Kuhlmann JD, Bachmann HS, Link T, Wimberge P, Kröber E, Thomssen C, Mallé B, Bethmann D, Vetter M, Kantelhardt EJ (2019) Association of caspase 8 polymorphisms -652 6N InsDel

and Asp302His with progression-free survival and tumor infiltrating lymphocytes in early breast cancer. Sci Rep 9: 12594. https://doi.org/10.1038/s41598-019-47601-x

Lagunin A, Stepanchikova A, Filimonov D, Poroikov V (2000) PASS: Prediction of activity spectra for biologically active substances. Bioinformatics 16(8): 747–748. https://doi.org/10.1093/bioinformatics/16.8.747

Lappano R, Sebastiani A, Cirillo F, Rigiracciolo DC, Galli GR, Curcio R, Malaguarnera R, Belfiore A, Cappello AR, Maggiolini M (2017) The lauric acid-activated signaling prompts apoptosis in cancer cells. Cell Death Discov 3: 17063. https://doi.org/10.1038/cddiscovery.2017.63

Mahwish, Imran M, Naeem H, Hussain M, Alsagaby SA, Abdulmonem WA, Mujtaba A, Abdelgawad MA, Ghoneim MM, El-Ghorab AH, Selim S, Jaouni SKA, Mostafa EM, Yehuala TF (2025) Antioxidative and anticancer potential of luteolin: A comprehensive approach against a wide range of human malignancies. Food Sci Nutr 13: e4682. https://doi.org/10.1002/fsn3.4682

Morshed AKMH, Paul S, Hossain A, Basak T, Hossain S, Hasan MM, Hasibuzzaman MA, Rahaman TI, Mia MAR, Shing P, Sohel M, Bibi S, Dey D, Biswas P, Hasan MN, Ming LC, Tan CS (2023) Baicalein as a promising anticancer agent: A comprehensive analysis on molecular mechanisms and therapeutic perspectives. Cancers 15(7): 2128. https://doi.org/10.3390/cancers15072128

Mutiah R, Safina NAN, Janaloka NA, Zahira SR, Annisa R, Febriyanti AP, Maimunah S (2024) The potential compounds in *Lansium parasiticum* leaf extract for breast cancer therapy: Metabolite profiling, pharmacological network analysis and in silico validation. Asian Pac J Cancer Prev 25(11): 3831–3840. https://doi.org/10.31557/APJCP.2024.25.11.3831

Mwangi JW, Kiragu D, Chaka B (2024) Phytochemical screening, FTIR and GCMS analysis of *Cucurbita pepo* seeds cultivated in Kiambu county, Kenya. Heliyon 10(9): e30237. https://doi.org/10.1016/j.heliyon.2024.e30237

Nagoor Meeran MF, Javed H, Taee HA, Azimullah S, Ojha SK (2017) Pharmacological properties and molecular mechanisms of thymol: Prospects for its therapeutic potential and pharmaceutical development. Front Pharmacol 8: 380. https://doi.org/10.3389/fphar.2017.00380

NCBI (2025a) PubChem Compound Summary for CID 40490600, Luteolin 7-O-beta-D-glucuronide. National Center for Biotechnology Information. https://pubchem.ncbi.nlm.nih.gov/compound/Luteolin-7-O-beta-D-Glucuronide [Consulted 26 October, 2025].

NCBI (2025b) PubChem Compound Summary for CID 44258405, Baicalein 6-glucuronide. National Center for Biotechnology Information. https://pubchem.ncbi.nlm.nih.gov/compound/Baicalein-6-glucuronide [26 October, 2025].

NCBI (2025c) PubChem Compound Summary for CID 185914, Dihydroresveratrol. National Center for Biotechnology Information. https://pubchem.ncbi.nlm.nih.gov/compound/Dihydroresveratrol [26 October, 2025].

Pegram M, Jackisch C (2023) Estrogen/HER2 receptor crosstalk in breast cancer: Combination therapies to improve outcomes for patients with hormone receptor-positive/HER2-positive breast cancer. NPJ Breast Cancer 9: 45. https://doi.org/10.1038/s41523-023-00533-2

Pramely R, Raj TLS (2012) Prediction of biological activity spectra of a few phytoconstituents of *Azadirachta indica* A. Juss. J Biochem Tech 3(4): 375–379.

Pu X, Storr SJ, Zhang Y, Rakha EA, Green AR, Ellis IO, Martin SG (2017) Caspase-3 and caspase-8 expression in breast cancer: Caspase-3 is associated with survival. Apoptosis 22(3): 357–368. https://doi.org/10.1007/s10495-016-1323-5

Purkon DB, Fadhlillah FM, Maigoda TC, Iwo MI, Soemardji AA, Nadhifah A, Sudaryat Y (2022) Phytochemical, use in ethnomedicine, and therapeutic activities of *Marchantia* genus. J Vocat Health Stud 5(3): 174. https://doi.org/10.20473/jvhs.V5.I3.2022.174-185

Simanullang RH, Situmorang PC, Herlina M, Noradina, Silalahi B (2022) Cytochrome c expression by andaliman (*Zanthoxylum acanthopodium*) on cervical cancer histology. Pak J Biol Sci 25(1): 49–55. https://doi.org/10.3923/pjbs.2022.49.55

Siregar ES, Pasaribu N, Sofyan MZ (2021) Antioxidant activity of liverworts *Marchantia paleacea* Bertol. from North Sumatra, Indonesia. IOP Conf Ser Earth Environ Sci 713: 012061. https://doi.org/10.1088/1755-1315/713/1/012061

Situmorang PC, Wibowo S, Ilyas S, Sari RM, Nugraha AP, Ibrahim A, Fitrianita A, Abiyyu N, Syahputra RA (2025a). *Rhodomyrtus tomentosa* attenuates HER2 expression and modulates apoptotic pathways in DMBA-induced breast carcinogenesis: *In vivo* and *in silico* insights. J Agric Food Res 24: 102360. https://doi.org/10.1016/j.jafr.2025.102360

Situmorang PC, Wibowo S, Sari RM, Nugraha AP, Ibrahim A, Fitrianita A, Abiyyu N, Ilyas S, Syahputra RA (2025b) Nephroprotective effects of *Rhodomyrtus tomentosa* in 7,12-dimethylbenz[a]anthracene (DMBA)-induced nephrotoxicity: Computational and physiological analysis of cytokine expression. J Agric Food Res 23: 102155. https://doi.org/10.1016/j.jafr.2025.102155

Vazhappilly C, Amararathna M, Cyril A, Linger R, Matar R, Merheb M, Ramadan W, Radhakrishnan R, Rupasinghe H (2021) Current methodologies to refine bioavailability, delivery, and therapeutic efficacy of plant flavonoids in cancer treatment. J Nutr Biochem 108623. https://doi.org/10.1016/j.jnutbio.2021.108623

Velmurugan BK, Lin JT, Mahalakshmi B, Chuang YC, Lin CC, Lo YS, Hsieh MJ, Chen MK (2020) Luteolin-7-O-glucoside inhibits oral cancer cell migration and invasion by regulating matrix metalloproteinase-2 expression and extracellular signal-regulated kinase pathway. Biomolecules 10(4): 502. https://doi.org/10.3390/biom10040502

Von Minckwitz G, Huang CS, Mano MS, Loibl S, Mamounas EP, Untch M, Wolmark N, Rastogi P, Schneeweiss A, Redondo A, Fischer HH, Jacot W, Conlin AK, Arce-Salinas C, Wapnir IL, Jackisch C, DiGiovanna MP, Fasching PA, Crown JP, Geyer CE (2019) Trastuzumab emtansine for residual invasive HER2-positive breast cancer. N Engl J Med 380(7): 617–628. https://doi.org/10.1056/NEJMoa1814017

Wang J, Wu S (2023) Breast cancer: An overview of current therapeutic strategies, challenges, and perspectives. Breast Cancer Targets Ther 15(8): 721–730. https://doi.org/10.2147/BCTT.S432526

Zhu C, Fan F, Li CY, Xiong Y, Liu X (2024) Caspase-3 promotes oncogene-induced malignant transformation via EndoG-dependent Src–STAT3 phosphorylation. Cell Death Dis 15: 486. https://doi.org/10.1038/s41419-024-06884-3

AUTHOR CONTRIBUTION:

Contribution	Siregar ES	Situmorang PC	Pasaribu N	Hairima H	Hasibuan MR
Concepts or ideas	x	x			
Design	x	x			
Definition of intellectual content		x	x	x	
Literature search				x	x
Experimental studies		x		x	x
Data acquisition	x	x		x	x
Data analysis	x			x	x
Statistical analysis	x				
Manuscript preparation	x			x	
Manuscript editing	x		x		x
Manuscript review	x	x	x	x	x

Citation Format: Siregar ES, Situmorang PC, Pasaribu N, Hairima H, Hasibuan MR (2025) Profiling and potential of *Marchantia paleacea* Bertol. extract for breast anticancer candidate: GC-MS, LC-MS/MS, and *in silico* analysis. J Pharm Pharmacogn Res 13(s1): S371–S393. https://doi.org/10.56499/jppres25.2531_13.s1.371

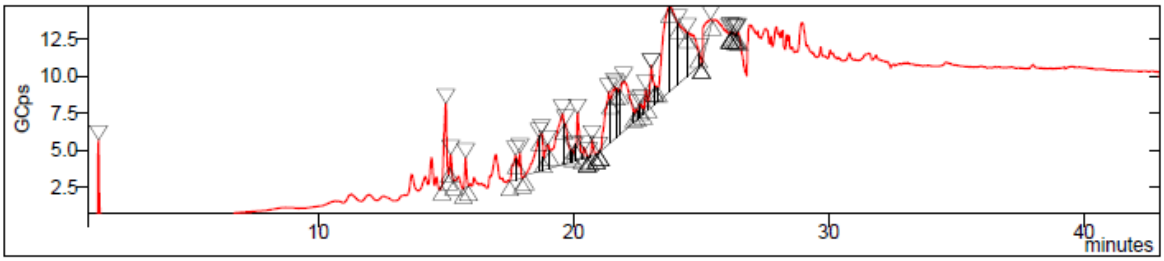
Publisher's Note: All claims expressed in this article are solely those of the authors and do not necessarily represent those of their affiliated organizations, or those of the publisher, the editors and the reviewers. Any product that may be evaluated in this article, or claim that may be made by its manufacturer, is not guaranteed or endorsed by the publisher.

Open Access: This article is distributed under the terms of the Creative Commons Attribution 4.0 International License (http://creativecommons.org/ licenses/by/4.0/), which permits use, duplication, adaptation, distribution and reproduction in any medium or format, as long as you give appropriate credit to the original author(s) and the source, provide a link to the Creative Commons license and indicate if changes were made.

Supplementary data

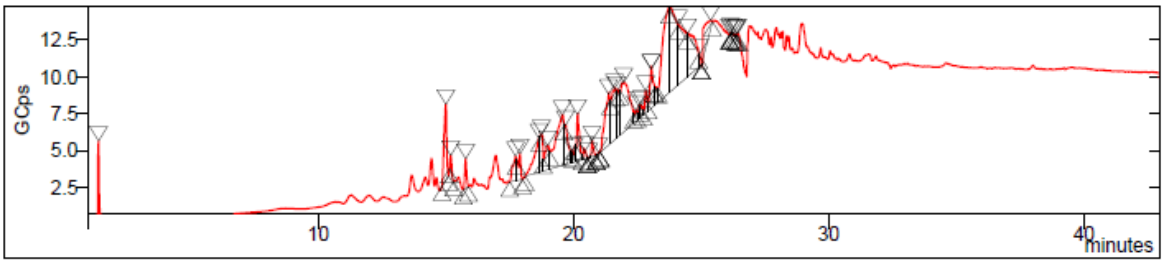
Print Date: 11 Dec 2023 15:01:24 Sample Report for marchantia paleacea.xms

Sample ID:	Marchantia Paleacea	Operator:	Mutia
Instrument ID:	Bruker GC/MS #1	Last Calibration:	None
Acquisition Date:	12/11/2023 12:18 PM	Data File:	...chantia paleacea.xms
Calculation Date:	12/11/2023 1:01 PM	Method:	...ta\uji fitokimia.mth
Inj. Sample Notes:	None		



Target Compounds

None



Unidentified Peaks

Quan Ions: RIC Spectrum Match Type: Normal-Forward
RF Used: None Match Thresh: 500

#	RT	Peak Name	Res Type	Area	Amount	R.Match
1	1.399	1,2-Ethanediol	TIC	1.687e+10	1.781	745
2	15.003	2,4-Hexadiene	TIC	3.645e+10	3.849	596
3	15.193	Thymol	TIC	4.717e+9	0.498	898
4	15.779	1-Undecanol	TIC	9.589e+9	1.013	776
5	17.731	n-Tridecan-1-ol	TIC	1.471e+10	1.553	806
6	17.908	Pentadecane	TIC	1.439e+10	1.519	883
7	18.652	Dodecanoic acid	TIC	3.331e+10	3.517	848
8	18.748	Dodecanoic acid	TIC	1.906e+10	2.013	862
9	18.989	1-Undecanol	TIC	2.013e+10	2.125	802
10	19.558	Dodecanoic acid	TIC	7.314e+10	7.723	813
11	19.683	Dodecanoic acid	TIC	2.749e+10	2.903	857
12	19.921	cis-9-Tetradecen-1-ol	TIC	4.521e+9	0.477	653
13	20.028	11-Hexadecen-1-ol, (Z)-	TIC	4.598e+9	0.486	866
14	20.157	1-Tridecene	TIC	2.428e+10	2.564	827
15	20.452	2-Dodecanone	TIC	4.802e+9	0.507	834
16	20.725	1-Tridecene	TIC	5.445e+9	0.575	761
17	20.991	No Match	Unk.	1.260e+8	0.013	----
18	21.373	Tetradecanoic acid	TIC	4.945e+10	5.222	864
19	21.602	Tetradecanoic acid	TIC	4.103e+10	4.333	871
20	21.695	Tetradecanoic acid	TIC	2.832e+10	2.990	875
21	21.968	Tetradecanoic acid	TIC	8.226e+10	8.687	881
22	22.433	n-Hexadecanoic acid	TIC	5.263e+9	0.556	596
23	22.564	2-Decanone	TIC	3.884e+9	0.410	762
24	22.664	1,6-Octadien-3-ol, 3,7-dimet	TIC	5.128e+9	0.541	576
25	22.824	2-Dodecanone	TIC	9.281e+9	0.980	705
26	23.040	Hexadecanoic acid, methyl es	TIC	2.702e+10	2.854	632
27	23.190	No Match	Unk.	8.434e+9	0.891	----

#	RT	Peak Name	Res Type	Area	Amount	R.Match
28	23.731	Dodecanoic acid	TIC	1.069e+11	11.288	796
29	23.793	Dodecanoic acid	TIC	9.580e+10	10.116	789
30	24.105	n-Decanoic acid	TIC	7.526e+10	7.947	739
31	24.462	n-Hexadecanoic acid	TIC	6.341e+10	6.695	675
32	24.942	n-Hexadecanoic acid	TIC	3.902e+9	0.412	653
33	25.374	n-Hexadecanoic acid	TIC	2.608e+10	2.754	656
34	26.155	Bicyclo[2.2.1]hept-5-en-2-ol	TIC	4.384e+8	0.046	519
35	26.264	No Match	Unk.	5.604e+8	0.059	----
36	26.337	No Match	Unk.	1.334e+8	0.014	----
37	26.391	Cyclohexanone, 2-nitro-	TIC	2.303e+8	0.024	545
38	26.427	Cyclohexanone, 2-nitro-	TIC	6.098e+8	0.064	626

No. 18-18-2.1/F- MU/SMM -SIG
Revisi : 1

REKAMAN PENGUJIAN LCMS/MS QTOF

Parameter Uji : Screening LCMS/MS QTOF
Library Uji : Natural Product *Library*
Metode Acuan : 18-18-2/MU/SMM-SIG
Tanggal Pengujian : 22 Agustus 2019

Penel	
Analis	Supervisor
Andreatian Refeldi	Drt Lulu Agus M.

No	No. Sampel	Matriks	Volume (mL)	Faktor Pengenceran	Volume Akhir (mL)	ESI	Hasil (Positif / Negatif)	Keterangan
1	908.R.3151 a	Ekstrak	1,0000	10	1	(+)	Positif	(3α,4β,5α)-4,5-Dihydro-4,5-dimethyl-3-(1-pyrrolyl)-furan-2(3H)-one
						(+)	Positif	Adenosine
						(+)	Positif	Dihydrogentianine
						(+)	Positif	Indole-3-acetonitrile-6-O-β-D-glucopyranoside
						(+)	Positif	Riboflavin (Vitamin B2)
						(+)	Positif	5,7-Dihydroxychromone
						(+)	Positif	Daidzin_1
						(+)	Positif	6-Gingerdione
						(+)	Positif	Myricomplanoside
						(+)	Positif	1-Carbomethoxy-β-carboline
						(+)	Positif	Luteolin-7-O-glucuronide
						(+)	Positif	2-Hydroxy-5-methyl-nypnone
						(+)	Positif	Baicalein-6-glucuronide
						(+)	Positif	Haematoxylin
						(+)	Positif	Myricetin 3',5'-dimethyl ether3-O-β-D-glucopyranoside
						(+)	Positif	5,6,7,3'-Tetrahydroxy-4'-methoxyisoflavone
						(+)	Positif	1,8-Dihydroxy-2,3,6-trimethoxyxanthone
						(+)	Positif	Pinocembrin_1
						(+)	Positif	Luteolin
						(+)	Positif	Sulfuretin
						(+)	Positif	Flavone
						(+)	Positif	Flavanthrinin
						(+)	Positif	Jaceosidin
						(-)	Positif	6-Isoinosine
						(-)	Positif	Gentialbetine
						(-)	Positif	2,4,5-Trihydroxybenzaldehyde
						(-)	Positif	p-Hydroxyphenol
						(-)	Positif	Vanillyl alcohol
						(-)	Positif	Guaiacol
						(-)	Positif	p-Tolualdehyde
						(-)	Positif	5,7-Dihydroxychromone
						(-)	Positif	Eupatin
						(-)	Positif	Luteolin-7-O-glucuronide
						(-)	Positif	5,7,8,4'-Tetrahydroxy flavone
						(-)	Positif	Mirificin
						(-)	Positif	(2R,3R)-3,5,7,2',6'-Pentahydroxy flavanone
						(-)	Positif	(3R)-4'-Methoxy-2',3,7-trihydroxy-Isoflavanone
						(-)	Positif	Kaempferol
						(-)	Positif	Baicalein-6-glucuronide
						(-)	Positif	Leucocyanidin
						(-)	Positif	d-Umbelin
						(-)	Positif	Eriodictyol-7-O-β-D-methyl-glucuronopyranoside
						(-)	Positif	Limocitrin-3-O-β-D-glucopyranoside
						(-)	Positif	2,4,7-Trihydroxy-9,10-dihydrophenanthrene
						(-)	Positif	Genistein
						(+)	Positif	3'-O-Methyltaxifolin
						(+)	Positif	(-)-Epiafzelechin-3-O-β-D-allopyranoside
						(-)	Positif	Pinocembrin_1
						(-)	Positif	Resokaempferol
						(-)	Positif	Dendrocandin E
						(-)	Positif	Dihydroresveratrol
						(-)	Positif	Irilone
						(-)	Positif	3,4',5-Trihydroxy-3',7-dimethoxyflavanone
						(-)	Positif	Flavanthrinin
						(-)	Positif	(R)-Prechrysophanol
2	908.R.3151 d	Ekstrak	1,0000	10	1	(+)	Positif	(3α,4β,5α)-4,5-Dihydro-4,5-dimethyl-3-(1-pyrrolyl)-furan-2(3H)-one
						(+)	Positif	Adenosine
						(+)	Positif	Dihydrogentianine
						(+)	Positif	Indole-3-acetonitrile-6-O-β-D-glucopyranoside
						(+)	Positif	Riboflavin (Vitamin B2)
						(+)	Positif	5,7-Dihydroxychromone
						(+)	Positif	Daidzin_1
						(+)	Positif	6-Gingerdione
						(+)	Positif	Myricomplanoside
						(+)	Positif	1-Carbomethoxy-β-carboline
						(+)	Positif	Luteolin-7-O-glucuronide
						(+)	Positif	2-Hydroxy-5-methyl-nypnone
						(+)	Positif	Baicalein-6-glucuronide
						(+)	Positif	Haematoxylin
						(+)	Positif	Myricetin 3',5'-dimethyl ether3-O-β-D-glucopyranoside
						(+)	Positif	5,6,7,3'-Tetrahydroxy-4'-methoxyisoflavone

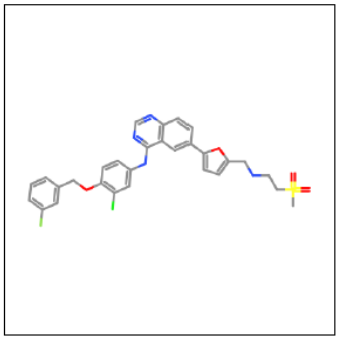
Page 1

No	No. Sampel	Matriks	Volume (mL)	Faktor Pengenceran	Volume Akhir (mL)	ESI	Hasil (Positif / Negatif)	Keterangan
						(+)	Positif	1,8-Dihydroxy-2,3,6-trimethoxyxanthone
						(+)	Positif	Pinocembrin_1
						(+)	Positif	Luteolin
						(+)	Positif	Sulfuretin
						(+)	Positif	Flavone
						(+)	Positif	Flavanthrinin
						(+)	Positif	Jaceosidin
						(-)	Positif	6-Isoinosine
						(-)	Positif	Gentiatibetine
						(-)	Positif	2,4,5-Trihydroxybenzaldehyde
						(-)	Positif	p-Hydroxyphenol
						(-)	Positif	Vanillyl alcohol
						(-)	Positif	Guaiacol
						(-)	Positif	p-Tolualdehyde
						(-)	Positif	5,7-Dihydroxychromone
						(-)	Positif	Euparin
						(-)	Positif	Luteolin-7-O-glucuronide
						(-)	Positif	5,7,8,4'-Tetrahydroxy flavone
						(-)	Positif	Mirificin
						(-)	Positif	(2R,3R)-3,5,7,2',6'-Pentahydroxy flavanone
						(-)	Positif	(3R)-4'-Methoxy-2',3',7-trihydroxy-isoflavanone
						(-)	Positif	Kaempferol
						(-)	Positif	Baicalein-6-glucuronide
						(-)	Positif	Leucocyanidin
						(-)	Positif	di-Umtatin
						(-)	Positif	Eriodictyol-7-O-β-D-methyl-glucuronopyranoside
						(-)	Positif	Limocitrin-3-O-β-D-glucopyranoside
						(-)	Positif	2,4,7-Trihydroxy-9,10-dihydrophenanthrene
						(-)	Positif	Genistein
						(-)	Positif	3'-O-Methyltaxifolin
						(-)	Positif	(-)-Epiafzelechin-3-O-β-D-allopyranoside
						(-)	Positif	Pinocembrin_1
						(-)	Positif	Resokaempferol
						(-)	Positif	Dendrocandin E
						(-)	Positif	Dihydroresveratrol
						(-)	Positif	Irilone
						(-)	Positif	3,4',5-Trihydroxy-3',7-dimethoxyflavanone
						(-)	Positif	Flavanthrinin
						(-)	Positif	(R)-Prechrysophanol
3	908.R.3152 a	Ekstrak	1,0000	10	1	(+)	Positif	Gentiatibetine
						(+)	Positif	2,4,6-Trihydroxyacetophenone-2,4-di-O-β-D-glucopyranoside
						(+)	Positif	Indole-3-acetonitrile-6-O-β-D-glucopyranoside
						(+)	Positif	Pinocembrin_1
						(+)	Positif	Astilbin
						(+)	Positif	Quercetin-3-O-β-D-glucuronide
						(+)	Positif	Luteolin-7-O-glucuronide
						(+)	Positif	Luteolin
						(+)	Positif	Baicalein-6-glucuronide
						(+)	Positif	Sulfuretin
						(+)	Positif	Kaempferol 3-O-β-D-glucuronopyranosyl methyl ester
						(+)	Positif	Caesalpins P
						(+)	Positif	2',7-Dihydroxy-4',5'-dimethoxyisoflavone
						(+)	Positif	Fawcettiine
						(+)	Positif	2,6-Di-tert-butyl-4-hydroxy toluene
						(+)	Positif	Flavanthrinin
						(-)	Positif	Cimidahurinine
						(-)	Positif	2,4,6-Trihydroxyacetophenone-2,4-di-O-β-D-glucopyranoside
						(-)	Positif	3-O-[β-D-Glucopyra-nosyl-(1→2)]-β-D-glucopyranosyl-kaempferol
						(-)	Positif	5,7,2'-Trihydroxy-flavanone-4'-O-β-D-glucoside
						(-)	Positif	Quercetin-3-O-β-D-glucuronide
						(-)	Positif	2,3,5,4'-Tetrahydroxystilbene-2-O-β-D-glucopyranoside
						(-)	Positif	5,7,8,4'-Tetrahydroxy flavone
						(-)	Positif	Luteolin-7-O-glucuronide
						(-)	Positif	Baicalein-6-glucuronide
						(-)	Positif	Kaempferol 3-O-β-D-glucuronopyranosyl methyl ester
						(-)	Positif	Kaempferol
						(-)	Positif	Dihydroresveratrol
						(-)	Positif	Genistein
						(-)	Positif	1,3,5-O-Tricaffeoyl-quinic acid
						(-)	Positif	Kaempferide
						(-)	Positif	(R)-Prechrysophanol
4	908.R.3152 d	Ekstrak	1,0000	10	1	(+)	Positif	Gentiatibetine
						(+)	Positif	2,4,6-Trihydroxyacetophenone-2,4-di-O-β-D-glucopyranoside
						(+)	Positif	Indole-3-acetonitrile-6-O-β-D-glucopyranoside
						(+)	Positif	Pinocembrin_1
						(+)	Positif	Astilbin
						(+)	Positif	Quercetin-3-O-β-D-glucuronide
						(+)	Positif	Luteolin-7-O-glucuronide
						(+)	Positif	Luteolin
						(+)	Positif	Baicalein-6-glucuronide
						(+)	Positif	Sulfuretin

No	No. Sampel	Matrika	Volume (mL)	Faktor Pengenceran	Volume Akhir (mL)	ESI	Hasil (Positif / Negatif)	Keterangan
						(+)	Positif	Kaempferol 3-O-β-D-glucuronopyranosyl methyl ester
						(+)	Positif	Caesalpins P
						(+)	Positif	2',7-Dihydroxy-4',5'-dimethoxyisoflavone
						(+)	Positif	Fawcettine
						(+)	Positif	2,6-Di-tert-butyl-4-hydroxy toluene
						(+)	Positif	Flavanthrinin
						(-)	Positif	Clmidahurinine
						(-)	Positif	2,4,6-Trihydroxyacetophenone-2,4-di-O-β-D-glucopyranoside
						(-)	Positif	3-O-[β-D-Glucopyra-nosyl-(1→2)]-β-D-glucopyranosyl-kaempferol
						(-)	Positif	5,7,2'-Trihydroxy-flavanone-4'-O-β-D-glucoside
						(-)	Positif	Quercetin-3-O-β-D-glucuronide
						(-)	Positif	2,3,5,4'-Tetrahydroxystilbene-2-O-β-D-glucopyranoside
						(-)	Positif	5,7,8,4'-Tetrahydroxy flavone
						(-)	Positif	Luteolin-7-O-glucuronide
						(-)	Positif	Baicalein-6-glucuronide
						(-)	Positif	Kaempferol 3-O-β-D-glucuronopyranosyl methyl ester
						(-)	Positif	Kaempferol
						(-)	Positif	Dihydroresveratrol
						(-)	Positif	Genistein
						(-)	Positif	1,3,5-O-Tricaffeoyl-quinic acid
						(-)	Positif	Kaempferide
						(-)	Positif	(R)-Prechrysophanol
5	908.R.3153 a	Ekstrak	1,0000	10	1	(+)	Positif	Adenosine
						(+)	Positif	Gentiatibetine
						(+)	Positif	Clmidahurinine
						(+)	Positif	2,4,6-Trihydroxyacetophenone-2,4-di-O-β-D-glucopyranoside
						(+)	Positif	Indole-3-acetonitrile-6-O-β-D-glucopyranoside
						(+)	Positif	Cyanidin 3,5-diglucoside_1
						(+)	Positif	7-O-α-L-Rhamnosyl-(1→3)-O-β-D-glucopyranosyl kaempferol
						(+)	Positif	Luteolin-7-O-[β-D-apiofuranosyl(1→6)]β-D-glucopyranoside
						(+)	Positif	Clerodendrin
						(+)	Positif	Patuletin-7-O-[6''-(2-methylbutyryl)]-glucoside
						(+)	Positif	Viscumneoside II
						(+)	Positif	Luteolin-7-O-glucuronide
						(+)	Positif	Robinetin
						(+)	Positif	Sulfuretin
						(+)	Positif	Baicalein-6-glucuronide
						(+)	Positif	Kaempferol 3-O-β-D-glucuronopyranosyl methyl ester
						(+)	Positif	Luteolin
						(+)	Positif	Caesalpins P
						(+)	Positif	Pinocembrin_1
						(+)	Positif	2,6-Di-tert-butyl-4-hydroxy toluene
						(+)	Positif	Flavanthrinin
						(-)	Positif	2,4,5-Trihydoxybenzaldehyde
						(-)	Positif	Clmidahurinine
						(-)	Positif	Sesamol
						(-)	Positif	2,4,6-Trihydroxyacetophenone-2,4-di-O-β-D-glucopyranoside
						(-)	Positif	p-Tolualdehyde
						(-)	Positif	Cyanin
						(-)	Positif	2''-Hydroxynaringenin
						(-)	Positif	6-Aldehydo-isoophio-pogonone A
						(-)	Positif	Kaempferol-3-O-β-D-glucoside-7-O-α-L-arabinofuranoside
						(-)	Positif	Luteolin-7-O-[β-D-apiofuranosyl(1→6)]β-D-glucopyranoside
						(-)	Positif	Dihydrokaempferol-5-O-β-D-glucopyranoside
						(-)	Positif	Schaftoside
						(-)	Positif	Isovitexin (Homovitexin)
						(-)	Positif	Eupanin
						(-)	Positif	Viscumneoside II
						(-)	Positif	Isoacteoside
						(-)	Positif	Luteolin-7-O-glucuronide
						(-)	Positif	Baicalein-6-glucuronide
						(-)	Positif	Kaempferol
						(-)	Positif	Dihydroresveratrol
						(-)	Positif	2,4,7-Trihydroxy-9,10-dihydrophenanthrene
						(-)	Positif	di-Umtatin
						(-)	Positif	Genistein
						(-)	Positif	1,3,5-O-Tricaffeoyl-quinic acid
6	908.R.3153 d	Ekstrak	1,0000	10	1	(+)	Positif	Adenosine
						(+)	Positif	Gentiatibetine
						(+)	Positif	Clmidahurinine
						(+)	Positif	2,4,6-Trihydroxyacetophenone-2,4-di-O-β-D-glucopyranoside
						(+)	Positif	Indole-3-acetonitrile-6-O-β-D-glucopyranoside
						(+)	Positif	Cyanidin 3,5-diglucoside_1
						(+)	Positif	7-O-α-L-Rhamnosyl-(1→3)-O-β-D-glucopyranosyl kaempferol
						(+)	Positif	Luteolin-7-O-[β-D-apiofuranosyl(1→6)]β-D-glucopyranoside

No	No. Sampel	Matriks	Volume (mL)	Faktor Pengenceran	Volume Akhir (mL)	ESI	Hasil (Positif / Negatif)	Keterangan
						(+)	Positif	Clerodendrin
						(+)	Positif	Patuletin-7-O-[6''-(2-methylbutyryl)]-glucoside
						(+)	Positif	Viscumneoside II
						(+)	Positif	Luteolin-7-O-glucuronide
						(+)	Positif	Robinetin
						(+)	Positif	Sulfuretin
						(+)	Positif	Baicalein-6-glucuronide
						(+)	Positif	Kaempferol 3-O-β-D-glucuronopyranosyl methyl ester
						(+)	Positif	Luteolin
						(+)	Positif	Caesalpins P
						(+)	Positif	Pinocembrin_II
						(+)	Positif	2,6-Di-tert-butyl-4-hydroxy toluene
						(+)	Positif	Flavanthrinin
						(-)	Positif	2,4,5-Trihydroxybenzaldehyde
						(-)	Positif	Clmidahurinine
						(-)	Positif	Sesamol
						(-)	Positif	2,4,6-Trihydroxyacetophenone-2,4-di-O-β-D-glucopyranoside
						(-)	Positif	p-Tolualdehyde
						(-)	Positif	Cyanin
						(-)	Positif	2'-Hydroxynaringenin
						(-)	Positif	6-Aldehydo-isopchio-pogonone A
						(-)	Positif	Kaempferol-3-O-β-D-glucoside-7-O-α-L-arabinofuranoside
						(-)	Positif	Luteolin-7-O-[6-O-apiofuranosyl(1→6)]β-D-glucopyranoside
						(-)	Positif	Dihydrokaempferol-5-O-β-D-glucopyranoside
						(-)	Positif	Schaftoside
						(-)	Positif	Isovitexin (Homovitexin)
						(-)	Positif	Eupatin
						(-)	Positif	Viscumneoside II
						(-)	Positif	Isoacteoside
						(-)	Positif	Luteolin-7-O-glucuronide
						(-)	Positif	Baicalein-6-glucuronide
						(-)	Positif	Kaempferol
						(-)	Positif	Dihydroresveratrol
						(-)	Positif	2,4,7-Trihydroxy-9,10-dihydrophenanthrene
						(-)	Positif	di-Umtatin
						(-)	Positif	Genistein
						(-)	Positif	1,3,5-O-Tricaffeoyl-quinic acid
7	QC Standar Caffeine 1 ppm					(+)	Positif	Caffeine
8	QC Standar Chloramphenicol 1 ppm					(-)	Positif	Chloramphenicol

Oral toxicity prediction results for input compound



Predicted LD50: 1500mg/kg

Predicted Toxicity Class: 4

1 2 3 4 5 6

Average similarity: 39.97%

Prediction accuracy: 23%

20% 40% 60% 80%

Name	CS(=O)(=O)CCNCC1=CC=C(O1
Molweight	581.06
Number of hydrogen bond acceptors	7
Number of hydrogen bond donors	2
Number of atoms	40
Number of bonds	44
Number of rotable bonds	11
Molecular refractivity	153.88
Topological Polar Surface Area	114.73
octanol/water partition coefficient(logP)	7.68

Toxicity Model Report

Copy Excel CSV PDF

Classification	Target	Shorthand	Prediction	Probability
Organ toxicity	Hepatotoxicity	dili	**Active**	0.80
Toxicity end points	Cytotoxicity	cyto	**Active**	0.76

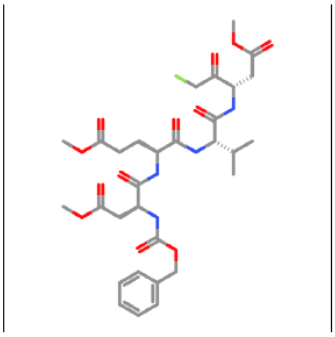
Toxicity targets

Possible binding to toxicity targets is shown below. For more information on the targets, please click on the individual abbreviations.

no binding probable binding

AA2AR	ADRB2	ANDR	AOFA	CRFR1	DRD3	ESR1	ESR2	GCR	HRH1	NR1I2	OPRK	OPRM	PDE4D	PGH1	PRGR

Oral toxicity prediction results for input compound



Predicted LD50: 920mg/kg

Predicted Toxicity Class: 4

1 2 3 4 5 6

Average similarity: 51.44%

Prediction accuracy: 67.38%

20% 40% 60% 80%

Name	CC(C)[C@@H](C(=O)N[C@@H](CC(=O)OC)C(=O)CF)NC[C@H](CCC(=O)OC)NC(=O)[C@H](CC(=O)OC)NC(=O)OCC
Molweight	668.67
Number of hydrogen bond acceptors	16
Number of hydrogen bond donors	4
Number of atoms	47
Number of bonds	47
Number of rotable bonds	27
Molecular refractivity	159.56
Topological Polar Surface Area	221.6
octanol/water partition coefficient(logP)	1.57

Toxicity Model Report

Copy Excel CSV PDF

Classification	Target	Shorthand	Prediction	Probability
Organ toxicity	Hepatotoxicity	dili	Inactive	0.84
Toxicity end points	Cytotoxicity	cyto	Inactive	0.65

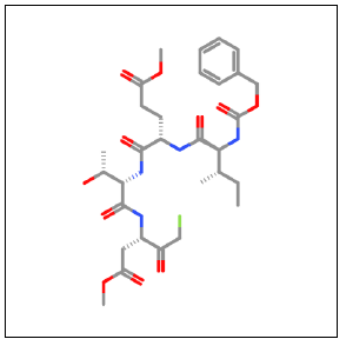
Toxicity targets

Possible binding to toxicity targets is shown below. For more information on the targets, please click on the individual abbreviations.

no binding probable binding

AA2AR	ADRB2	ANDR	AOFA	CRFR1	DRD3	ESR1	ESR2	GCR	HRH1	NR1I2	OPRK	OPRM	PDE4D	PGH1	PRGR

Oral toxicity prediction results for input compound



Predicted LD50: 300mg/kg

Predicted Toxicity Class: 3

1 2 3 4 5 6

Average similarity: 53.4%

Prediction accuracy: 67.38%

20% 40% 60% 80%

Name	CC[C@H](C)[C@@H](C(=O)N[C@@H](CCC(=O)OC)C(=O)N[C@([C@@H](C)O)C(=O)N[C@@H](CC(=O)OC)C(=O)CF)NC
Molweight	654.68
Number of hydrogen bond acceptors	15
Number of hydrogen bond donors	5
Number of atoms	46
Number of bonds	46
Number of rotable bonds	26
Molecular refractivity	159.43
Topological Polar Surface Area	215.53
octanol/water partition coefficient(logP)	1.78

Toxicity Model Report

Copy Excel CSV PDF

Classification	Target	Shorthand	Prediction	Probability
Organ toxicity	Hepatotoxicity	dili	Inactive	0.84
Toxicity end points	Cytotoxicity	cyto	Inactive	0.69

Toxicity targets

Possible binding to toxicity targets is shown below. For more information on the targets, please click on the individual abbreviations.

no binding probable binding

AA2AR	ADRB2	ANDR	AOFA	CRFR1	DRD3	ESR1	ESR2	GCR	HRH1	NR1I2	OPRK	OPRM	PDE4D	PGH1	PRGR